Effect of wall friction on oscillation of velocity at the head of the gravity current

Koue, Jinichi

(Citation)
Theoretical and Applied Mechanics Letters,13(3):100439

(Issue Date)
2023-05

(Resource Type)
journal article

(Version)
Version of Record

(URL)
https://hdl.handle.net/20.500.14094/0100482475

Theoretical and Applied Mechanics Letters 13 (2023) 100439

Contents lists available at ScienceDirect

Theoretical and Applied Mechanics Letters

journal homepage: www.elsevier.com/locate/taml

Letter

Effect of wall friction on oscillation of velocity at the head of the gravity current

Jinichi Koue

Graduate School of Maritime Sciences, Kobe University, Japan

ARTICLE INFO

Article history:
Received 18 December 2022
Revised 11 February 2023
Accepted 14 February 2023
Available online 17 February 2023

Keywords:
Gravity current
Velocity oscillations
Transition
Reynolds number
Wall friction

ABSTRACT

Velocity oscillations at the head of the gravity current were investigated in experiments and numerical simulations of a locked-exchange flow. A comparison of the experimental and numerical simulations showed that the depth and volume of the released fluid affected the oscillations in the velocity of the gravity current. At the initial stage, the head moved forward at a constant velocity, and velocity oscillations occurred. The head maximum thickness increased at the same time as the head, which did not have a round, and accumulated buoyant fluid due to the buoyancy effect intrusion force. The period of accumulation and release of the buoyant fluid was almost the same as that observed for the head movement velocity; the head movement velocity was faster when the buoyant fluid accumulated and slower when it was released. At the viscous stage, the forward velocity decreased proportionally to the power of 1/2 of time, since the head was not disturbed from behind. As the mass concentration at the head decreased, the gravity current was slowed by the viscous stage in its effect. At the viscous stage, the mass concentration at the head was no longer present, and the velocity oscillations also decreased.

The gravity current is the flow of one fluid through another, caused by a relatively small difference in density between the fluids. In natural aquatic environments, such as lakes, oceans, and reservoirs, there are a myriad of possible sources of density differences, including temperature differences, salinity differences, suspended solids—both organic and inorganic—and combinations of these mechanisms [1]. In the area of human activity, gravity currents generated in the atmosphere and ocean may have buoyancy as their driving force, as a result of the accidental release and subsequent flotation of industrial pollutants. Thus, the gravity current is a very complex flow that is ubiquitous in nature and human activity, and its study is as diverse in purpose as it is in the manifestation of the flow itself.

In the ocean, gravity currents have a density interface where temperature and salinity change in discontinuities of densities, preventing material transportation in a perpendicular direction. This has an impact on the supply of nutrition and oxygen. Before and after the gravity current passes, the material cycle around the fluid changes. As a result, it is critical to forecast how the marine environment will change. Gravity currents have been studied extensively, both experimentally [2,3] and numerically [4–6]. Many experiments to generate gravity currents have been carried out by opening the gate in the water tank to investigate the front speed and the mixture of the gravity current [7].

The gravity current generally consists of the head with unsteady and strong vortex motion and a relatively steady flow behind the head. Many theoretical and experimental studies have been conducted to clarify the properties of the steady flow part. The accuracy and consistency of the developed model are checked using the experimental data of the lock-exchange in the straight channel, lateral flow in the open channel, and mass exchange in the cavity [8]. The evolution of the local mixing dynamics along a lock-exchange gravity current propagating over a mild slope was statistically investigated and they showed the characteristic of the slumping and initial stages of the current's propagation [9].

According to Simpson [1] and Hallworth et al. [10], the growth process of the gravity current can be classified into three major stages. Immediately after the sluice gate is opened, the first stage appears, in which the leading edge of the gravity current maintains a constant velocity; followed by a transition to the second stage, in which the leading edge begins to decelerate and the inertial force and gravity reach equilibrium; and finally, to the third stage, in which the effect of viscous friction becomes dominant and further deceleration occurs [11]. Hoult [12] conducted experiments on

E-mail address: koue@maritime.kobe-u.ac.jp

https://doi.org/10.1016/j.taml.2023.100439

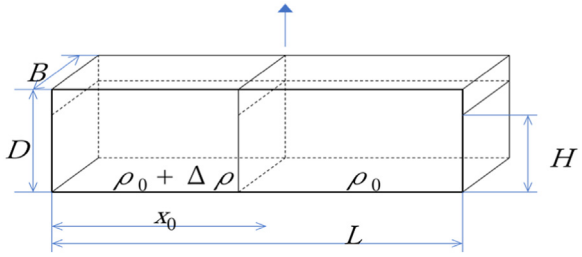

Fig. 1. A schematic diagram of lock-exchange flow.

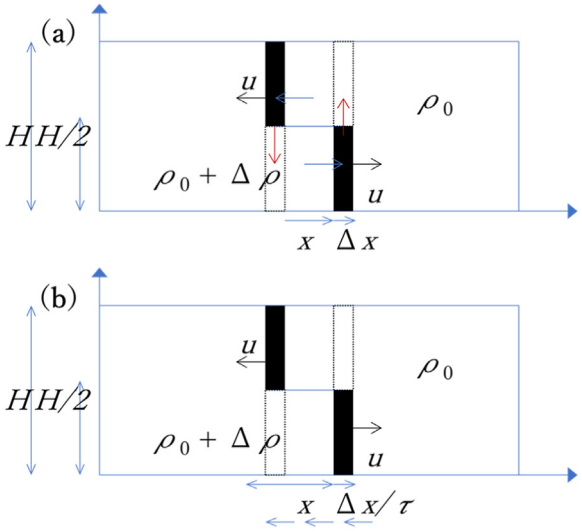

Fig. 2. (**a**) Initial stage of gravity current. (**b**) Viscous stage of the gravity current.

the diffusion of heavy oil when a constant supply of heavy oil was kept on the water, and a third stage emerged in which viscous friction became dominant even though the heavy oil was traveling along the free surface. Didden and Maxworthy [13] observed the behavior of the leading edge of a channel with parallel sidewalls in which a constant supply of low-density fluid was applied, and they reported that a third stage appeared as well. However, analysis of the head part with unsteady motion is still insufficient and many unknowns remain.

The purpose of this study is to analyze how the velocity at the head of the gravity current varies. The variation in the structure of the head of the gravity current was investigated theoretically by applying the box-model, experimentally by using the water tank, and numerically by using the slope-limiting scheme. This experiment included the condition of no disturbance to the head from behind during the viscous stage.

The theoretical, experimental, and numerical investigation of gravity current propagation in a long channel of length L and water depth H was conducted. Figure 1 depicts a water tank with $L = 4000$ mm length and $D = 60$ mm depth. The gate was placed from the edge of the water tank to the position of distance x_0=L/2, the fluid with the density of ρ_0 was placed in one area partitioned by the gate, and the fluid with the density of ρ_0+$\Delta\rho$ was placed in the other. As for the density difference of the fluid, the case of several percent salt water was used to do this experiment. The behavior and structure of the head of the gravity current after the gate was opened was examined.

Figure 2a depicts the initial stage after the gate was opened. The fluid exchange occurred in relation to the symmetry position of the gate, the height of the gravity current became half its initial value, and it progressed. The amount of energy change between the state after the gate is opened and the state where the head of the gravity current advances distance x is taken into account. The amount of the change in potential energy, ΔP, by the gravity current is given by:

$$\Delta P = -\frac{1}{4}\Delta\rho\Delta x \cdot gH^2, \tag{1}$$

where $\Delta\rho$ is the difference in density, Δx is the difference in distance, g is the gravitational acceleration, and H is the water depth.

It is equal to the potential energy when a heavy fluid falls only half of the initial height and is exchanged for a light fluid.

The change in kinetic energy of the head, ΔK, can be expressed as:

$$\Delta K = \rho_0 \cdot \Delta x \cdot H \cdot v^2, \tag{2}$$

where ρ is the density of fluid in the head, and v is the characteristic velocity.

Assuming that dynamic energy is conserved and that all decreasing potential energy is used to generate kinetic energy:

$$\Delta P + \Delta K = 0. \tag{3}$$

Therefore, the front speed is given by:

$$v = \frac{1}{2}\sqrt{\frac{\Delta\rho}{\rho_0}gH}. \tag{4}$$

The viscous stage is depicted in Fig. 2b, where friction is created between the progressing fluid and the bottom of the wall. When a rectangular area of fluid distance of x in length moves the distance of Δx along the bottom of the wall, the change in dissipative energy, ΔD, can be written in the form of:

$$\Delta D = \tau x \Delta x, \tag{5}$$

where shearing stress τ is regarded to be proportional to the velocity:

$$\tau = \mu\frac{1}{H}\frac{\mathrm{d}x}{\mathrm{d}t}, \tag{6}$$

and μ denotes the viscosity coefficient of the fluid.

If the dissipative energy is entirely due to a decrease in potential energy, the moving distance x is given by:

$$x = \frac{1}{\sqrt{2}}\sqrt{\frac{\Delta\rho}{\mu}gH^3t}. \tag{7}$$

When the viscosity on the bottom wall becomes dominant, the front speed decreases as the moving distance is proportional to the time to the power of 1/2.

As previously stated, gravity current progresses due to the potential energy of the density difference, and in terms of energy conversion, gravity current development stages can be divided into two stages: the initial stage and the viscous stage.

An acrylic and aluminum water tank with L = 4000 mm, B = 100 mm in width, and D = 60 mm in depth was used as shown in Fig. 1. The tank was placed on a horizontal stand, and a partition plate was attached that opens and closes vertically. A plastic plate was used as the divider, and a guide was attached to the plate to allow it to move smoothly up and down. The gate was placed at the middle of the tank, the fluid with the density of ρ_0 was placed in one area partitioned by the gate, and the fluid with the density of ρ_0+$\Delta\rho$ was placed in the other. The less dense fluid ρ0 was fresh water and the denser fluid ρ_0+$\Delta\rho$ was a solution of water and sodium chloride with dye. A gravimeter and refractometer were used to measure the density ratio. The divider was opened to generate a density flow. A digital video camera was used to measure the position of the tip of the density flow. The location of the tip of the gravity current was determined by obtaining the luminance values from the image of the tip of the gravity current, finding the midpoint between fresh water and salt water with red

dye, and using the threshold line as the tip location. The images were captured by a computer, and the elapsed time at each 50 mm distance from the sluice gate was recorded. The water depth H was set to 25 mm, and the density differences between the two fluids are 1%, 2%, and 4%, respectively. The Reynolds numbers ($\mathrm{Re} = UH/\gamma$) (γ is the kinematic viscosity of the fluid; the representative length as the water depth H, the representative velocity as the propagation velocity of the internal shallow water wave $U = \sqrt{g'H}$) were 1233, 1743, and 2465, in that order.

The governing equations are the Navier-Stokes equation for an inhomogeneous and incompressible fluid, the continuity equation, and the solute transport equation are the governing equations.

All variables were non-dimensionalized with the representative length as the water depth H, the representative velocity as the propagation velocity of the internal shallow water wave $U = \sqrt{g'H}$, and the representative time as $T = H/U$.

The Reynolds number $\mathrm{Re} = UH/\gamma$ and the diffusion parameter of the density $Rs = UH/\gamma$, and the Froude number $Fn = U/\sqrt{g'H}$, are included as dimensionless numbers, where κ is the molecular diffusion coefficient of the solute, and γ is the kinematic viscosity of the fluid and $Fn = 1.0$.

The density of a fluid becomes dimensionless in two steps. The initial density is the representative density, and the change from the representative density is nondimensionalized by the initial density difference. Bousinessq approximation is used as follows.

The non-dimensionalized density variation is expressed as:

$$\rho_s = \frac{\rho - \rho_0}{\Delta\rho}. \tag{8}$$

Governing equations: The Navier-Stokes equations for viscous fluids with density change is shown by:

$$\frac{\partial(\rho u)}{\partial t} + \nabla\cdot(\rho uu) = -\nabla\varphi + \mathrm{Re}^{-1}\nabla^2 u - \rho_s F_n^{-2} k. \tag{9}$$

The continuity equation for incompressible fluids is expressed by:

$$\nabla\cdot u = 0. \tag{10}$$

The transport equation for the density of the medium is described by:

$$\frac{\partial\rho_s}{\partial t} + \nabla\cdot(\rho_s u) = Rs^{-1}\nabla^2\rho_s, \tag{11}$$

where u is the velocity vector of the medium flow, t is the time, k is a unit vector in the vertical direction, φ is the change in pressure with respect to the hydrostatic pressure of the medium, and ρ_s is the change in density.

For an accurate representation of small density difference, the density variation relative to the initial density difference was used as the primitive variable, that is, $\rho_s = (\rho - \rho_0)/\Delta\rho$, so that the non-dimensional density variations are described as $\rho\rho_0 = -0.5$ for the denser fluid and $\rho_0 = -0.5$ for that with less density; as a result, the variation of the density is between −0.5 and 0.5. The location of the tip of the gravity current was determined by obtaining the density value ($\rho_0 = 0$) from the contour map of the tip of the gravity current, finding the midpoint between fresh water and salt water with red dye, and using the threshold line as the tip location.

The simulation conditions were matched to the experimental conditions. The initial length of the simulation domain was $L/H = 160$, the grid space was $\Delta x/H = \Delta y/H = 0.05$, and the time increment was set at $\Delta t/T = 0.005$, the initial density difference was $\Delta\rho/\rho_0 = 0.01$, 0.02, and 0.04. The Reynolds numbers were 1233, 1743, and 2465, respectively. The non-dimensional parameter of the diffusion of solute Rs was 10^5.

The governing equations were expanded into components of the Cartesian coordinate system and discretized based on the finite volume method. The components of the velocity calculation vector were staggered at the center of the cell surface, and the pressure and density were defined at the center of the cell. The spatial derivatives included in the governing equations were approximated by a second-order accurate central difference. The values at points in space other than the defining point were evaluated by the arithmetic mean of the values at adjacent defining points. As for the advective term of the transport equation of the density and the advective term of the Navier-Stokes equation was applied by the slope limiting scheme compared with the QUICK method [14], in addition to the central difference.

In order to prevent numerical oscillation for the advective term of the transport equation of the density and the advective term of the Navier-Stokes equation, the slope- limiting scheme was applied to solve the equation under very weak density diffusion conditions. No slip conditions of flow velocities were imposed at the side and bottom boundaries. For the top surface, a free-slip condition was imposed.

At the wall boundary, the condition that the diffusion velocity of the medium was zero was imposed as followed,

$$n\cdot\nabla\rho_s = 0, \tag{12}$$

the no-slip condition for velocity was imposed as follows:

$$u = 0, \tag{13}$$

and the free-slip condition was imposed as the following equations:

$$u_n = 0, \tag{14}$$

and

$$n\cdot\nabla u_t = 0, \tag{15}$$

where u_n and u_t were the normal and tangential components at the wall surface of the velocity, respectively.

The slope limiting scheme was applied to one-dimensional advection equation.

The one-dimensional advection equation is given by:

$$\frac{\partial \boldsymbol{f}}{\partial \boldsymbol{t}} + c\frac{\partial \boldsymbol{f}}{\partial \boldsymbol{x}} = 0. \tag{16}$$

The finite volume method is used to digitalize this equation, which is written in the form of:

$$\left(f_i^{n+1} - f_i^n\right)\Delta x + \left(F_{i+\frac{1}{2}} - F_{i-\frac{1}{2}}\right) = 0. \tag{17}$$

The value f is updated by:

$$f_i^{n+1} = f_i^n - \frac{F_{i+\frac{1}{2}} - F_{i-\frac{1}{2}}}{\Delta x}. \tag{18}$$

The average value of f is given by:

$$f_i^n = \frac{1}{\Delta x}\int_{x_{i-\frac{1}{2}}}^{x_{i+\frac{1}{2}}} f(x)\mathrm{d}x, \tag{19}$$

where, function $f(x)$ is approximated by the straight line, which is given by:

$$f(x) = f_i + a_i(x - x_i),\ \ x_i - \frac{1}{2}\Delta x < x < x_i + \frac{1}{2}\Delta x, \tag{20}$$

and the flux passing through cell boundaries F is shown by:

$$F_{i\pm\frac{1}{2}} = \int_{t^n}^{t^{n+1}} cf\left(t,\ x_{i\pm\frac{1}{2}}\right)\mathrm{d}t. \tag{21}$$

Considering the monotonous condition, which is given by: and the inequality concerning the slope is obtained as follows:

$$|a_i - a_{i-1}| \le 2\left|a_{i-\frac{1}{2}}\right|. \tag{23}$$

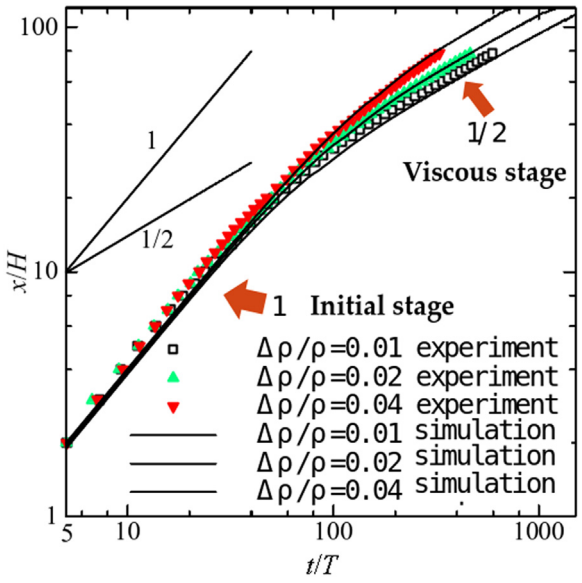

Fig. 3. Comparison of the position of the head of a gravity current between experiment and simulation.

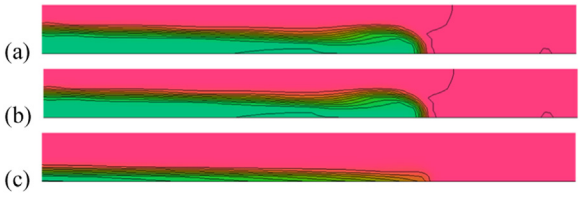

Fig. 4. Contour maps of density of gravity currents at (**a**) $t/T = 20$, (**b**) $t/T = 80$, and (**c**) $t/T = 200$ (Re=1233) (count of levels 21, increment in levels 0.1, minimum level −1, maximum level 1).

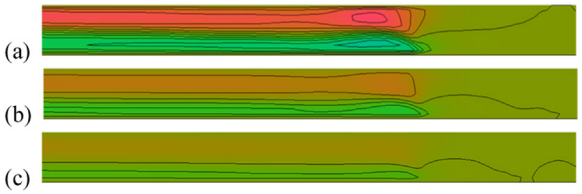

Fig. 5. Contour maps of horizontal velocity of gravity currents at (**a**) $t/T = 20$, (**b**) $t/T = 80$, and (**c**) $t/T = 200$ (Re=1233) (count of levels 21, increment in levels 0.1, minimum level −1, maximum level 1).

$a_{i-1/2}$ is the slope between f_{i-1} and f_i. In order to satisfy the condition, the slope is limited until it is sufficient.

Figure 3 depicts the logarithmic relationship between the position of the head of the gravity current and the time in the simulation. The results of experiments and simulation agreed well. Both the experimental and simulation results showed that the front speed advanced at a constant rate at the initial stage, then slowed; finally, dominated by the viscosity, the front decelerated with the time to the power of 1/2 when no disturbance from behind came to the head.

Figures 4–7 shows contour maps of density, horizontal and vertical velocity, and the pressure of the gravity currents at (a) $t/T = 20$, initial stage; (b) $t/T = 80$, transitional stage; and (c) $t/T = 200$ ($Re = 1233$), viscous stage, in the case of 1% initial density difference. The contour interval is 1/10 of the initial density difference. As for the contour map, the count of levels is 21, increment in levels is 0.1, minimum level is -1, and maximum level is 1 in each case of density, velocity, and pressure. At time $t/T = 20$, the head of the gravity current expanded. At time $t/T = 80$, which was between the initial stage and viscous stage, the height and mass concentration of the head part decreased. At time $t/T = 200$, the swelling of the head had stopped, and the head part had flattened. The head moved at a constant rate when the mass was concentrated at the head. The front speed decreased with the time to the power of 1/2 when the mass concentration at the head no longer existed.

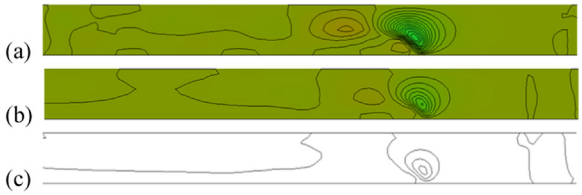

Fig. 6. Contour maps of vertical velocity of gravity currents at (**a**) $t/T = 20$, (**b**) $t/T = 80$, and (**c**) $t/T = 200$ (Re=1233) (count of levels 21, increment in levels 0.1, minimum level −1, maximum level 1).

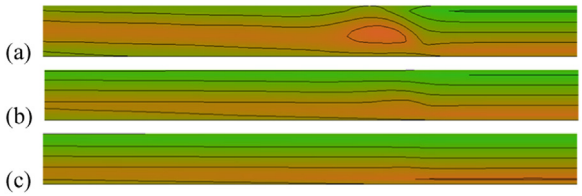

Fig. 7. Contour maps of pressure of gravity currents at (**a**) $t/T = 20$, (**b**) $t/T = 80$, and (**c**) $t/T = 200$ (Re=1233) (count of levels 21, increment in levels 0.1, minimum level −1, maximum level 1).

As for the 1% initial density difference, around time $t/T = 45$, the initial stage changed to the transitional stage, which was between the initial and viscous stages, as observed in the experiment. The transitional stage changed to the viscous stage around time $t/T = 125$. Furthermore, as for the case of the initial density difference of 2%, the initial stage changed to the transitional stage around time $t/T = 55$. The transitional stage changed to the viscous stage around $t/T = 175$. Concerning the 4% initial density difference, the initial stage shifted to the transitional stage around time $t/T = 75$. The transitional stage changed to the viscous stage around time $t/T = 210$.

In the initial stage after the opening of the sluice gate, gravity flow with half of the initial thickness travels at a constant velocity, but the leading edge of the gravity current swells to about the initial thickness, and immediately after that, the interface becomes narrow and sloped. In the transitional stage, the gravity current becomes thinner, the interface becomes almost horizontal, and the head swelling decreases. In the viscous stage, the dye at the head becomes thinner.

In the initial stage, the interface is inclined as a result of the collapsed tip of the gravity flow, while in the viscous stage; the interface is horizontal because its thickness decreases uniformly while remaining rectangular. Therefore, this difference in the shape of the interface is considered to affect the transition to the transitional stage. The fact that the leading edge of the density interface rises at a large angle to the wall is a direct effect of the no-slip condition of velocity at the viscous boundary, and the viscous condition causes the transition stage to self-similarity. This transition stage is considered to occur when the overall thickness of the gravity flow becomes as thin as the thickness of the boundary layer at the wall.

The change in Reynolds number and dimensionless time of the transition point were investigated. As shown in Fig. 8, the transition point was defined as the intersection of a straight line at the initial stage, where the front speed advanced at a constant speed, and one at the viscous stage, where the moving distance was proportional to the time to the power of 1/2. Furthermore, each straight line was obtained using the least-squares method for Reynolds numbers 50, 200, 500, 1116, 1620, 1900, and 2358.

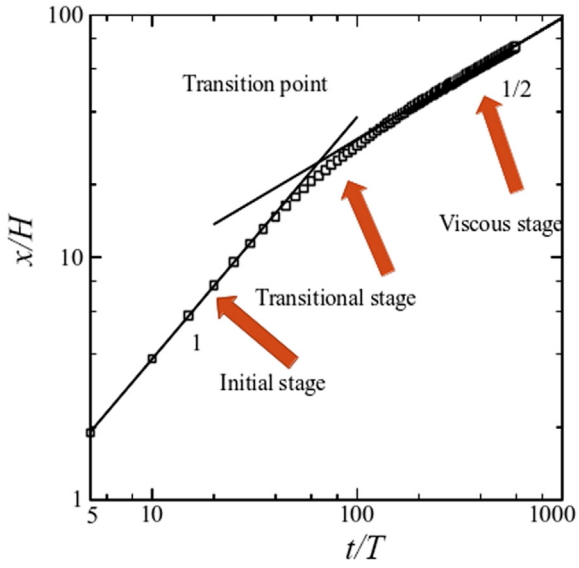

Fig. 8. The position of the head of a gravity current with time in the computation in logarithmic scale (Re=1233).

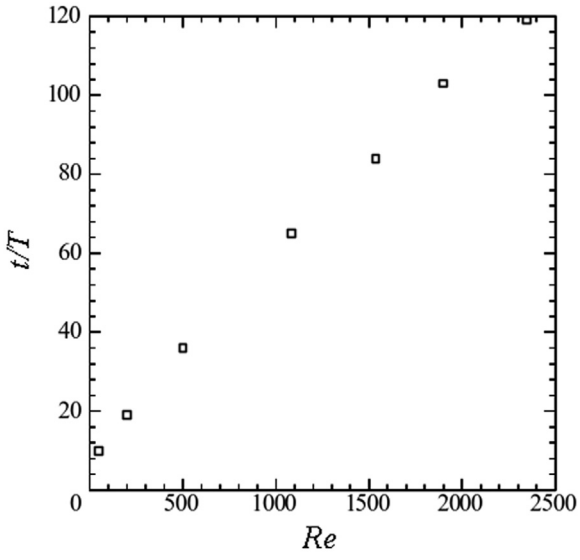

Fig. 9. The time variation of the position of a gravity current in the computation showing the effect of Reynolds number.

As a result of the graph in Fig. 9, it was discovered that the dimensionless time of the transition point from the initial to the viscous stage was proportional to the Reynolds number.

The fluctuation of the speed at the head of the gravity currents was investigated. Figure 10 shows the time change of the front speed at the head of the gravity currents of $Re = 1233$ in the simulation. Figure 11 is an expanded view of part of Fig. 10. As shown in Fig. 11a, the front speed fluctuated in microscopic areas at around $t/T = 64$, although the average front speed was constant at the initial stage. This showed that the front speed at the initial stage of the microscopic areas was unstable. Figure 11b shows the comparison between the slope-limiting method and QUICK method. Using both schemes, the period was found to be 0.2 around $t/T = 64$. The transition point was at $t/T = 80$, as shown in Fig. 8. According to Fig. 10, the fluctuation of the front speed increased to the peak at about that time. Moreover, it was approximately dimensionless at time $t/T = 110$ of change to a viscous stage in Fig. 10. Here, the front speed fluctuation started to calm down at approximately $t/T = 110$, as shown in Fig. 8. It was considered that the

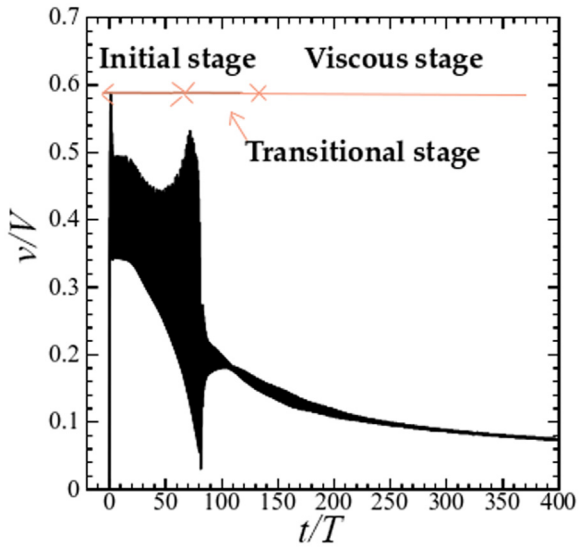

Fig. 10. The time change of the front speed of the gravity currents in the simulation ($Re = 1233$).

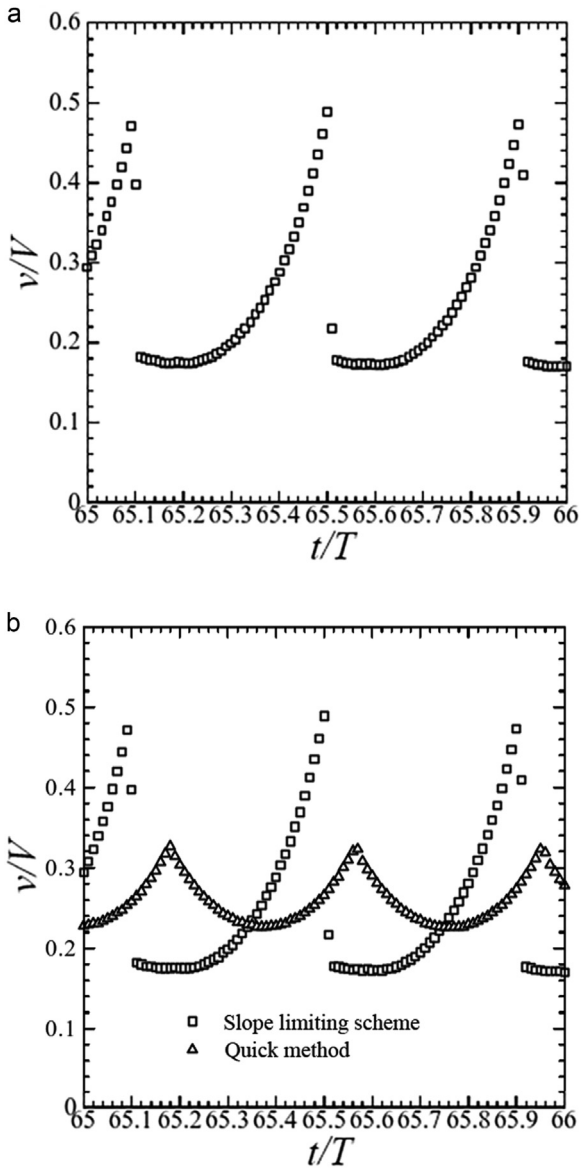

Fig. 11. (**a**) An enlarged graph of Fig. 8 at around $t/T = 64$ ($Re = 1233$), (**b**) comparison between slope-limiting scheme and QUICK method.

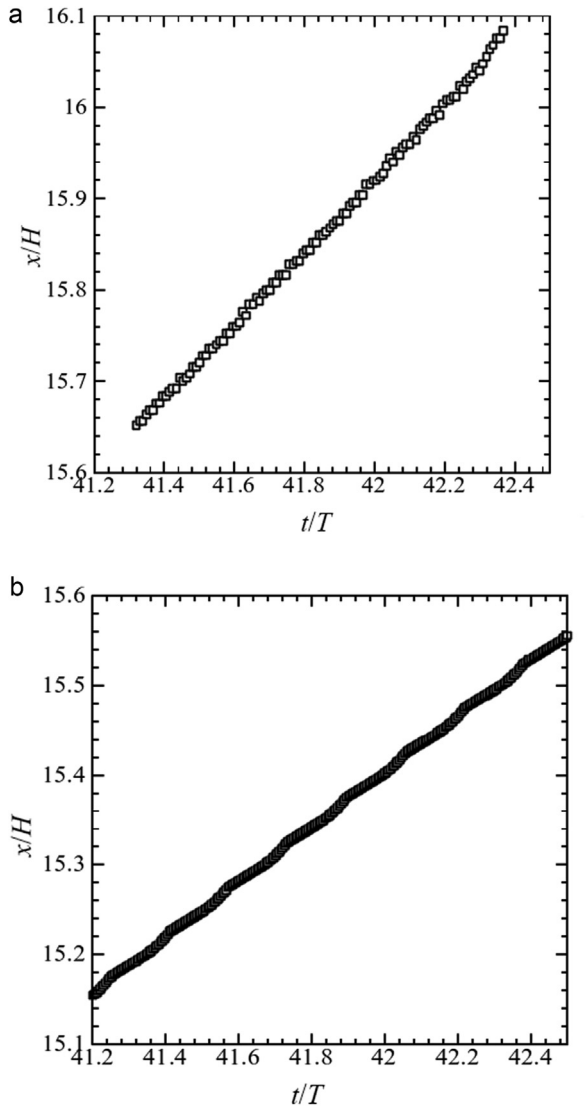

Fig. 12. The time variation of the position of the head of the gravity current at the initial stage (**a**) experiment, (**b**) simulation.

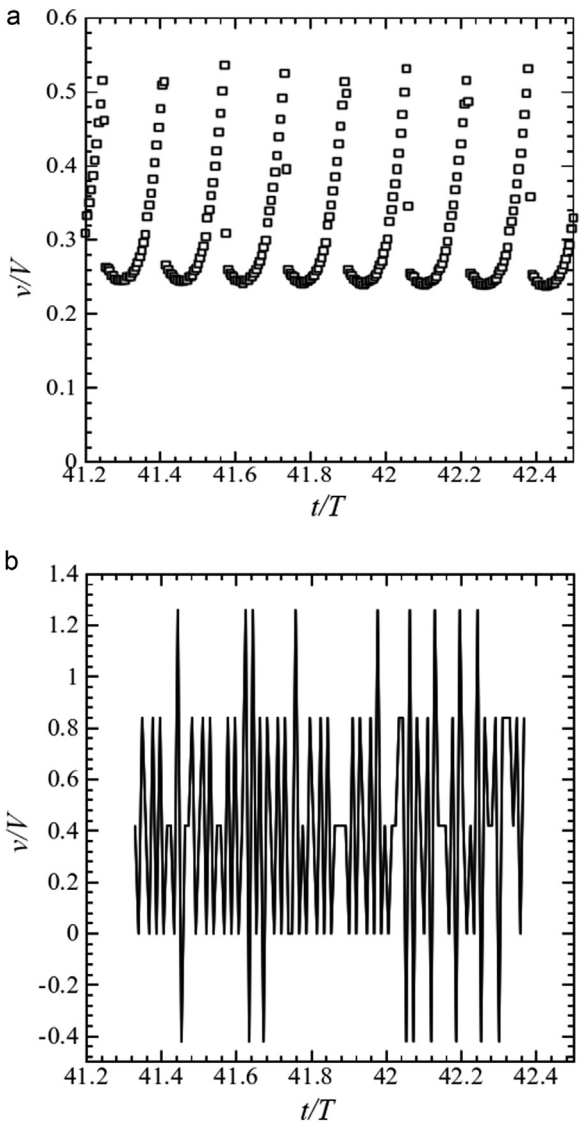

Fig. 13. The time variation of the velocity of the head of the gravity current at the initial stage (**a**) experiment; (**b**) simulation.

front speed at the viscous stage, where it decreased with the time to the power of 1/2, was stable.

Figures 12 and 13 show the time variation of the position and velocity of the head of the gravity current at the initial stage in the experiment and numerical simulation, respectively. The figures show that the velocity of the gravity current in the initial stage fluctuated periodically in both the experiments and numerical simulations. Figure 14 shows the experimental, numerical, and schematic diagrams of the tip height of the gravity current, and Fig. 15 shows the time variation of the tip height of the gravity current obtained by the numerical calculation. It was observed that the height fluctuation was large by the transitional stage, $t/T = 100$. The maximum tip thickness increased as soon as the tip of the gravity current without a round accumulated buoyant fluid due to the intrusion force caused by the buoyancy effect. This accumulation of buoyant fluid was considered to be caused by the higher velocity of the stationary part of the flow than that of the tip. The buoyancy effect was the result of the buoyant fluid entering the tip up to its limit (interfacial shear force), accumulating vorticity at the tip, and then re-leasing it as a vortex when it reached its limit. The tip would release buoyant fluid as a vortex. When the maximum tip thickness equaled the steady state thickness, the tip would start to accumulate buoyant fluid again. The period of accumulation and the re-lease of the buoyant fluid were almost the same as that observed for the tip movement velocity.

The dynamic structure of the head of the gravity current was investigated by the theory, experiment, and the simulation in the range of the Reynolds number 50–2500. The slope limiting scheme was used to prevent numerical oscillations in the density transport equation and the advective term of the Navier-Stokes equation.

An examination was carried out on the transition of the gravity current in the developmental stage without the influence of the wall of the water tank.

1. The front advanced at a constant speed during the initial stage and decelerated with a time to power of 1/2 during the viscous stage.
2. At the initial stage, the gravity current caused a mass concentration at the head. The gravity current decelerated due to the influence of viscosity as the head's mass concentration decreased. At the viscous stage, mass concentration at the head was no longer present.
3. Fluctuation of the front speed occurred at the initial stage. This fluctuation in-creased to a peak at the transition, then abruptly decreased when the viscous stage began.

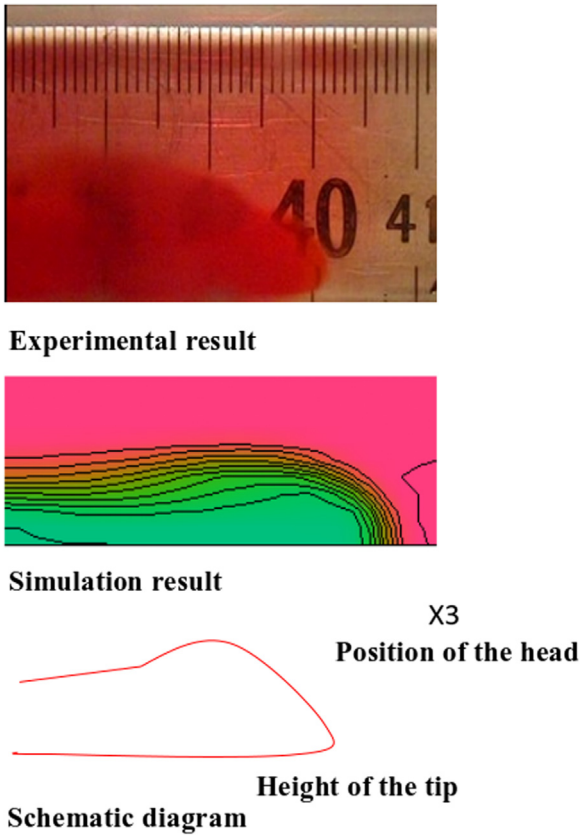

Fig. 14. The experimental, numerical, and schematic diagrams of the height of the tip of the gravity current.

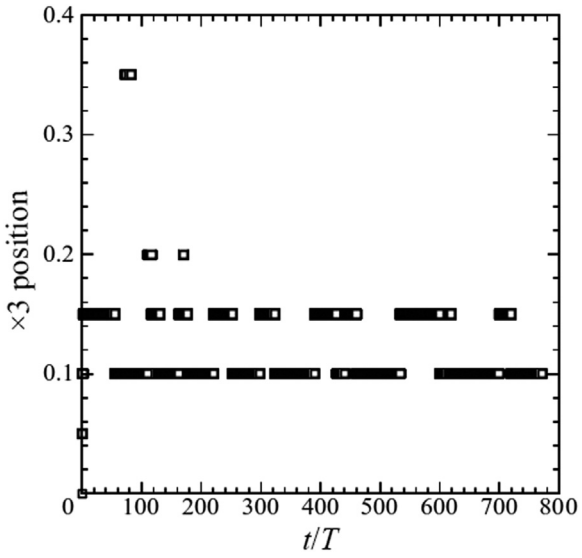

Fig. 15. The time variation of the tip height of the gravity current in the simulation.

4. The maximum tip thickness increased as soon as the tip of the gravity current without a round accumulated buoyant fluid due to the intrusion force caused by the buoyancy effect from the initial stage the transitional stage. This accumulation of buoyant fluid was considered to be caused by the higher velocity of the stationary part of the flow than that of the tip.
5. The buoyancy effect was the result of the buoyant fluid entering the tip up to its limit (interfacial shear force), accumulating vorticity at the tip, and then releasing it as a vortex when it reached its limit. The tip would release buoyant fluid as a vortex up. When the maximum tip thickness equaled the steady state thickness, the tip would start to accumulate buoyant fluid again. The period of accumulation and release of the buoyant fluid was almost the same as that observed for the tip movement velocity.

Anoxia of the bottom layer in enclosed bays is an environmental problem because it kills benthic organisms and has a wide range of effects due to wind and tidal fluctuations. In particular, anoxia of the bottom layer in harbor waters is becoming more serious, and the development of density stratification is one of the causes. A technique to promote vertical mixing by discharging buoyant jets into the bottom layer has been proposed as a remedial measure, and the impact of buoyant jets on the bay scale has been reported in impact predictions.

The present study suggested that the structure of the head of the gravity current transitioned from the initial to the viscous stage, and that velocity fluctuations occurred significantly up to the transitional stage, which should be taken into account in the impact predictions. The flow from the coastal area to the bay should also be taken into account, and the behavior of the buoyant jet near the outlet and the effect on the density stratification brought about by the jet should be considered. In addition, for closed water bodies, where bottom layer anoxia is a problem due to the development of density stratification, it is possible to accurately predict the effect of buoyant jets released near the density interface on the density distribution .

Declaration of Competing Interest

The authors declare that they have no known competing financial interests or personal relationships that could have appeared to influence the work reported in this paper.

Acknowledgments

This research did not receive any specific grant from funding agencies in the public or commercial.

References

[1] J.E. Simpson, Gravity Currents in the Environment and the Laboratory, 2nd ed., Cambridge University Press, Cambridge, UK, 1997.
[2] C. Cenedese, R. Nokes, J. Hyatt, Lock-exchange gravity currents over rough bottoms, Environ. Fluid Mech. 18 (2018) 59–73.
[3] J.O. Shin, S.B. Dalziel, P.F. Linden, Gravity currents produced by lock exchange, J. Fluid Mech. 521 (2004) 1–34.
[4] M. Darabian, E. Khavasi, A. Eyvazian, et al., Numerical simulation of stratifed intrusive gravity current in three dimensional state due to the presence of particles using large eddy simulation method, J. Braz. Soc. Mech. Sci. Eng. 43 (2021) 257.
[5] A. Kokkinos, P. Prinos, Numerical experiments of partial-depth colliding gravity currents using LES, Environ. Fluid Mech. 22 (2022) 1081–1105.
[6] B.A. Farenzena, J.H. Silvestrini, Gravity currents front velocity uncertainty, Comput. Fluids 232 (2022) 105209.
[7] N. Baba, S. Okamura, T. Fukuba, Structure of head of gravity current, J. Soc. Nav. Archit. Jpn. 1998 (1998) 197–205.
[8] S. Mahmodinia, M. Javan, Vortical structures, entrainment and mixing process in the lateral discharge of the gravity current, Environ. Fluid Mech. 21 (2021) 1035–1067.
[9] J. Pelmard, S. Norris, H. Friedrich, Turbulent density transport in the mixing layer of an unsteady gravity current, Adv. Water Resour. 154 (2021) 103963.
[10] M.A. Hallworth, A.J. Hogg, H.E. Huppert, Effects of external flow on compositional and particle gravity currents, J. Fluid Mech. 359 (1998) 109–142.
[11] J.W. Rottman, J.E. Simpson, Gravity currents produced by instantaneous releases of a heavy fluid in a rectangular channel, J. Fluid Mech. 135 (1983) 95–110.
[12] D.P. Hoult, Oil spreading on the sea, Annu. Rev. Fluid Mech. 4 (1972) 341–368.
[13] N. Didden, T. Maxworthy, The viscous spreading of plane and axisymmetric gravity currents, J. Fluid Mech. 121 (1982) 27–42.
[14] B.P. Leonard, A stable and accurate convective modelling procedure base on quadratic upstream interpolation, Comput. Methods Appl. Mech. Eng. 19 (1979) 59–98.